MOLECULAR AND CELLULAR BIOLOGY
2023, VOL. 43, NO. 5, 223–240
https://doi.org/10.1080/10985549.2023.2205344

Taylor & Francis
Taylor & Francis Group

RESEARCH ARTICLE

OPEN ACCESS Check for updates

# EPRS1 Controls the TGF-β Signaling Pathway via Interaction with TβRI in Hepatic Stellate Cell

**Ina Yoon,* Ji Ae Song,* Ji Hun Suh, Sulhee Kim, Jonghyeon Son, Jong Hyun Kim, Song Yee Jang, Kwang Yeon Hwang, Myung Hee Kim, Sunghoon Kim**

[a]Institute for Artificial Intelligence and Biomedical Research, Medicinal Bioconvergence Research Center, Yonsei University, Incheon, Republic of Korea
[b]Yonsei Institute of Pharmaceutical Sciences, College of Pharmacy, Yonsei University, Incheon, Republic of Korea
[c]Department of Biotechnology, College of Life Sciences and Biotechnology, Korea University, Seoul, Republic of Korea
[d]New Drug Development Center, Daegu-Gyeongbuk Medical Innovation Foundation, Daegu, Republic of Korea
[e]Department of Biochemistry, School of Medicine, Catholic University of Daegu, Daegu, Republic of Korea
[f]Microbiome Convergence Research Center, Korea Research Institute of Bioscience and Biotechnology (KRIBB), Daejeon, Korea Research Republic of Korea
[g]Core Research Facility & Analysis Center, KRIBB, Daejeon, Republic of Korea
[h]College of Medicine, Gangnam Severance Hospital, Yonsei University, Seoul, Republic of Korea

**ABSTRACT** Glutamyl-prolyl-tRNA synthetase 1 (EPRS1) is known to associated with fibrosis through its catalytic activity to produce prolyl-tRNA. Although its catalytic inhibitor halofuginone (HF) has been known to inhibit the TGF-β pathway as well as to reduce prolyl-tRNA production for the control of fibrosis, the underlying mechanism how EPRS1 regulates the TGF-β pathway was not fully understood. Here, we show a noncatalytic function of EPRS1 in controlling the TGF-β pathway and hepatic stellate cell activation via its interaction with TGF-β receptor I (TβRI). Upon stimulation with TGF-β, EPRS1 is phosphorylated by TGF-β-activated kinase 1 (TAK1), leading to its dissociation from the multi-tRNA synthetase complex and subsequent binding with TβRI. This interaction increases the association of TβRI with SMAD2/3 while decreases that of TβRI with SMAD7. Accordingly, EPRS1 stabilizes TβRI by preventing the ubiquitin-mediated degradation of TβRI. HF disrupts the interaction between EPRS1 and TβRI, and reduces TβRI protein levels, leading to inhibition of the TGF-β pathway. In conclusion, this work suggests the novel function of EPRS1 involved in the development of fibrosis by regulating the TGF-β pathway and the antifibrotic effects of HF by controlling both of EPRS1 functions.

**KEYWORDS** glutamyl-prolyl-tRNA synthetase 1, transforming growth factor receptors, halofuginone

## INTRODUCTION

Hepatic fibrosis is a chronic and progressive disease characterized by the accumulation of excessive extracellular matrix (ECM) in the liver.[1–3] Unlike a normal wound repair and regeneration process, repeated liver injury induced by various stimuli such as alcohol, western diets, viruses and toxins leads to progressive fibrotic responses and excessive production of ECM proteins, especially collagen.[3] Hepatic stellate cells (HSCs) play a key role in the development of hepatic fibrosis.[4] In response to damage-associated molecular patterns (DAMPs) released from the damaged hepatocytes, HSCs are activated and transdifferentiated to myofibroblast-like cells. These transdifferentiated cells enhance fibrogenesis, contractility, and inflammation leading to hepatic fibrosis. HSCs are the main collagen-producing cells within the liver and collagen production of HSCs is regulated by the transforming growth factor-beta (TGF-β) signaling pathway.[3,5]



Address correspondence to Sunghoon Kim, sunghoonkim@yonsei.ac.kr.

*These authors contributed equally to this work.

**Received** 4 October 2022
**Revised** 20 February 2023
**Accepted** 28 March 2023

The canonical TGF-β signaling pathway is initiated upon the binding of the TGF-β ligand with TGF-β receptor II (TβRII). This interaction leads to the recruitment of TGF-β receptor I (TβRI), and the activated receptor complex phosphorylates receptor-regulated SMADs (R-SMADs; SMAD2 and SMAD3). The activated R-SMADs form a trimeric complex with the co-SMAD (SMAD4) and translocate to the nucleus for the transcriptional control of target genes.[6,7] The TGF-β signaling pathway is negatively regulated by inhibitory SMAD (I-SMAD; SMAD7) through several mechanisms. I-SMAD competes with R-SMADs for TβRI interaction, recruits the E3 ligases or phosphatases to degrade or inactivate TβRI, respectively, and downregulates TβRI localization to the plasma membrane.[8,9]

Glutamyl-prolyl-tRNA synthetase 1 (EPRS1) is one of aminoacyl-tRNA synthetases (ARSs) that mediate the covalent linkage between amino acids to their cognate tRNAs for protein synthesis.[10–12] EPRS1 has three domains: glutamyl-tRNA synthetase 1 (EARS1), prolyl-tRNA synthetase 1 (PARS1) and three repeats of the WHEP domain that links EARS1 and PARS1. EARS1 and PARS1 catalyze glutamate and proline, respectively, to their cognate tRNAs. EPRS1, along with other seven ARSs (leucyl-tRNA synthetase 1 (LARS1), isoleucyl-tRNA synthetase 1 (IARS1), methionyl-tRNA synthetase 1 (MARS1), lysyl-tRNA synthetase 1 (KARS1), aspartyl-tRNA synthetase 1 (DARS1), arginyl-tRNA synthetase 1 (RARS1) and glutaminyl-tRNA synthetase 1 (QARS1)), and three auxiliary factors (aminoacyl tRNA synthetase complex interacting multifunctional protein 1, 2, and 3 (AIMP1, 2, and 3)) form a large complex called the multi-tRNA synthetase complex (MSC).[13–15] It is well-known that MSC components dissociate from the MSC in response to various stimuli and then perform noncatalytic functions which are related to disease conditions.[16–18]

Halofuginone (HF) is a derivative of febrifugine, an active compound of *Dichroa febrifuga* used as an antimalarial drug in traditional Chinese medicine.[19] Early studies about HF activities revealed that HF decreases collagen levels, promotes amino acid starvation response, and inhibits the phosphorylation of R-SMADs in response to TGF-β.[20–24] However, they could not suggest its mechanism because the target of HF had not been identified. After PARS1 has been identified as a molecular target of HF,[25–27] its ability to modulate collagen levels and amino acid starvation response is understood to be mediated by PARS1 catalytic activity regulation. Nevertheless, how HF regulates R-SMADs phosphorylation is not well understood.

The role of EPRS1 in fibrotic diseases has been investigated in cardiac, pulmonary, and hepatic fibrosis.[28–30] Other than catalytic activity producing prolylated tRNA (Pro-tRNA) that is required for the synthesis of fibrosis-inducing proline-rich proteins such as collagen and latent-transforming growth factor beta-binding protein 2 (LTBP2),[30] noncatalytic functions of EPRS1 controlling transcription of genes encoding ECM proteins such as collagen and fibronectin via signal transducer and activator of transcription 6 (STAT6) have been suggested.[28,29] However, the role of EPRS1 in regulating the canonical TGF-β signaling pathway has not been investigated, although the effects of HF on R-SMADs are well studied. Here, we suggest TGF-β-dependent noncatalytic function of EPRS1 modulating the interaction of TβRI, R-SMADs, and I-SMAD to control TGF-β signal transduction, and the effect of HF on the interaction, which would be implicated in hepatic fibrosis.

## RESULTS

**EPRS1 non-catalytically regulates the TGF-β signaling pathway.** To investigate the role of EPRS1 in the TGF-β signaling pathway and its effect on HSC activation and hepatic fibrosis, we established LX-2 cells stably expressing Flag-EPRS1 or shEPRS1 in the presence of doxycycline. Upon TGF-β stimulation, cells overexpressing Flag-EPRS1 proteins showed an increase in the phosphorylation of SMAD2 and increase in the levels of HSC activation marker α-smooth muscle actin (α-SMA)[31] and collagen compared with control cells (Fig. 1A). In addition, cells suppressing EPRS1 proteins using shEPRS1 showed a decrease in SMAD2 phosphorylation and decrease in the levels of α-SMA

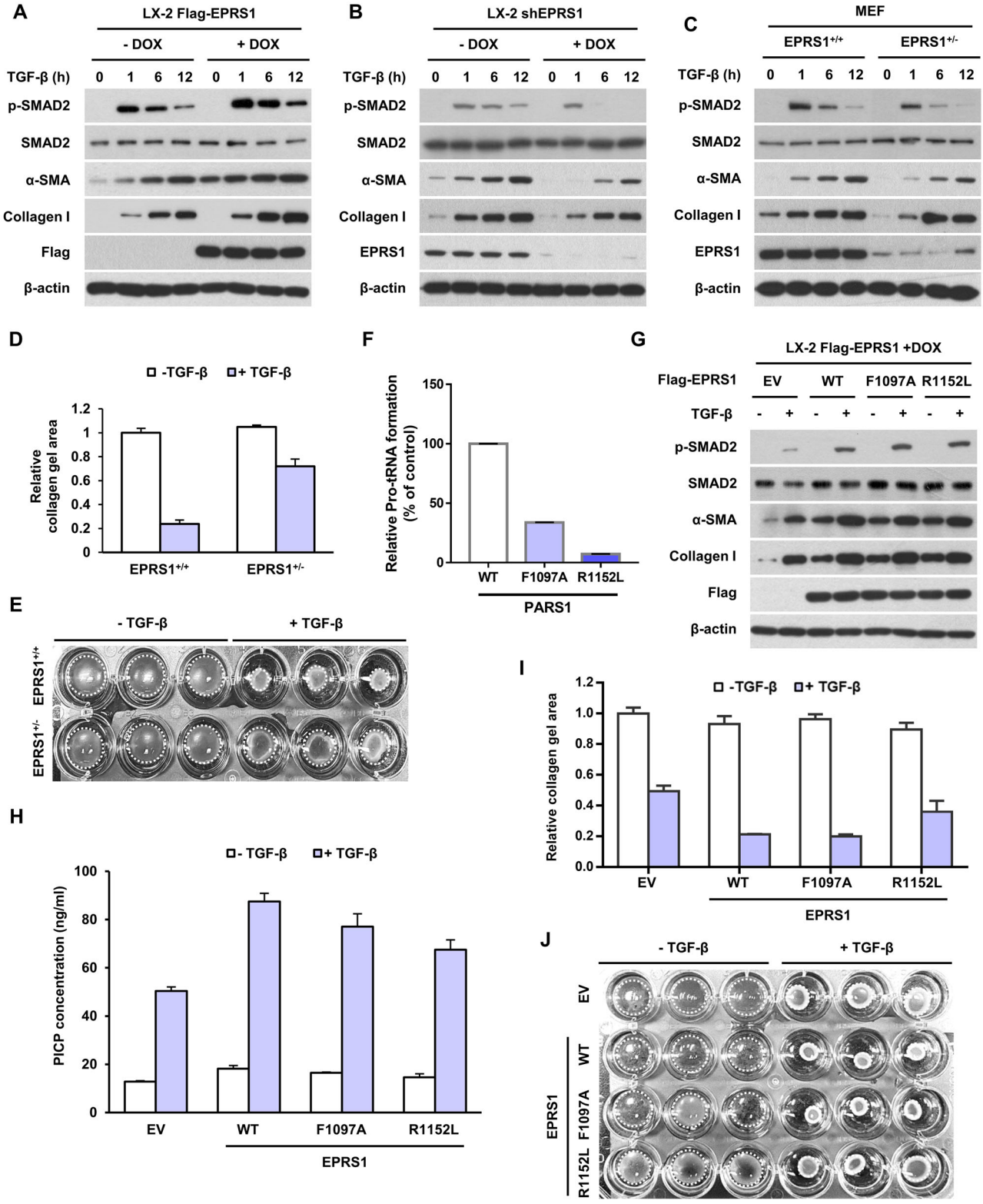


**FIG. 1** Involvement of noncatalytic function of EPRS1 in TGF-β-induced fibrosis. (A) LX-2 cells stably expressing Flag-EPRS1 in the presence of doxycycline were incubated with TGF-β for the indicated time. Cell lysates were prepared and the levels of the indicated proteins were detected through immunoblot assay. β-actin was used as a loading control. DOX, doxycycline. (B) LX-2 cells stably expressing shEPRS1 in the presence of doxycycline were incubated with TGF-β for the indicated time. Cell lysates were prepared and the levels of the indicated proteins were determined by immunoblot assay. (C) Mouse embryonic fibroblasts (MEFs) from *EPRS1* wild-type (*EPRS1*$^{+/+}$) and heterozygous (*EPRS1*$^{+/-}$) mice were incubated with TGF-β for the indicated time. Cell lysates were prepared and the levels of the indicated proteins were determined by immunoblot assay. (D and E) MEFs from *EPRS1*$^{+/+}$ and *EPRS1*$^{+/-}$ mice were mixed with collagen and incubated in the absence or presence of TGF-β for 12 h. Relative collagen gel size was determined (D) based on the white dotted circle (E) ($n = 3$, mean ± SEM). (F) Wild-type (WT) His-PARS1 and mutant His-PARS1 (F1097A and R1152L) were purified and catalytic activities of

(Continued on next page)

and collagen (Fig. 1B), suggesting the positive correlation between the protein levels of EPRS1 and SMAD2 phosphorylation and levels of α-SMA and collagen. Mouse embryonic fibroblasts (MEFs) obtained from the *EPRS1* wild-type (*EPRS1*$^{+/+}$) and heterozygous (*EPRS1*$^{+/-}$) mice also showed EPRS1-dependent control of SMAD2 phosphorylation, and α-SMA and collagen levels (Fig. 1C). In addition, *EPRS1*$^{+/-}$ MEFs exhibited decreased contractility compared to *EPRS1*$^{+/+}$ MEFs in the presence of TGF-β, as determined by collagen gel contraction assay (Fig. 1D and E). These results suggest that EPRS1 positively regulates the TGF-β signaling pathway and HSC activation.

Since EPRS1 is known to modulates collagen levels through its PARS1 catalytic activity, we investigated the contribution of catalytic or noncatalytic activities of EPRS1 to the TGF-β signaling pathway by using EPRS1 mutants. To obtain catalytically defective EPRS1 mutants, we introduced F1097A or R1152L mutations to EPRS1 based on the previous study.[26] We confirmed PARS1 catalytic activities of these mutants in an *in vitro* assay using purified proteins and radioactive isotope-labelled proline. PARS1 F1097A and R1152L proteins showed decreased or defective prolylation activities, respectively (Fig. 1F). Then, SMAD2 phosphorylation along with α-SMA and collagen levels were monitored in LX-2 cells stably expressing EPRS1 wild-type (WT), R1097A, or R1152L. Cells overexpressing EPRS1 mutants showed increased SMAD2 phosphorylation along with increased levels of α-SMA and collagen compared to the empty vector control group (Fig. 1G), suggesting the involvement of the noncatalytic activity of EPRS1 in TGF-β pathway activation. Next, we measured the levels of procollagen type I carboxy-terminal propeptide (PICP) in the culture media by ELISA. Results revealed that compared to the empty vector control group, cells overexpressing EPRS1 mutants produced higher levels of collagen; however, it was lower when compared to collagen produced by cells overexpressing WT EPRS1 (Fig. 1H), implying that both noncatalytic and catalytic activities of EPRS1 are involved in regulating collagen production. In addition, *EPRS1*$^{+/-}$ MEFs overexpressing EPRS1 mutants showed increased contractility compared to negative control group (Fig. 1I and J). Considering that *α-SMA* and collagen family genes are the target of the TGF-β pathway, these results suggest that EPRS1 noncatalytically modulates the TGF-β pathway and HSC activation.

**EPRS1 interacts with TβRI in a TGF-β-dependent manner.** To determine the mechanism by which EPRS1 regulates the TGF-β pathway, we tested proteins working in the TGF-β pathway for their ability to interact with EPRS1. When coimmunoprecipitation was performed with proteins involved in the canonical TGF-β pathway (TβRI, TβRII, SMAD2, SMAD3, SMAD4, and SMAD7), EPRS1 interacts with TβRI, and this interaction was increased in the presence of TGF-β (Fig. 2A). Moreover, TβRI showed no interaction with AARS1 (Fig. 2B), implying that among ARSs, EPRS1 specifically interacts with TβRI. We confirmed this interaction again in an endogenous system of LX-2 cells (Fig. 2C). EPRS1 F1097A and R1152L mutants were also able to interact with TβRI in a TGF-β-dependent manner, suggesting that these mutations had little effect on its interaction with TβRI (Fig. 2D). When monitoring TGF-β-dependent changes in subcellular localization of EPRS1, EPRS1 was localized to the membrane fraction along with TβRI upon stimulation with TGF-β (Fig. 2E). Immunofluorescence images staining EPRS1 also showed that EPRS1 was located in the plasma membrane in a TGF-β-dependent manner (Fig. 2F).

We then prepared EPRS1 fragments (EARS1, WHEP, and PARS1) based on structural information to determine the TβRI-interacting domain of EPRS1. Results showed that the PARS1 domain of EPRS1 was responsible for its interaction with TβRI (Fig. 3A).

**FIG. 1** Legend (Continued)
them were determined using [$^3$H]proline in an *in vitro* assay. The radioactive labelling of tRNA was quantified using a liquid scintillation counter (LSC) ($n = 3$, mean ± SEM). (G) LX-2 cells stably expressing the indicated protein in the presence of doxycycline were incubated in the absence or presence of TGF-β for 12 h. Cell lysates were prepared and the levels of the indicated proteins were determined by immunoblot assay. (H) MEFs from *EPRS1*$^{+/-}$ mice were transfected with the indicated plasmids and incubated in the absence or presence of TGF-β. Levels of collagens in culture media were quantified using ELISA detecting procollagen type I carboxy-terminal propeptide (PICP) ($n = 3$, mean ± SEM). (I and J) MEFs from *EPRS1*$^{+/-}$ mice were mixed with collagen and incubated in the absence or presence of TGF-β for 12 h. Relative collagen gel size was determined (I) based on the white dotted circle (J) ($n = 3$, mean ± SEM).

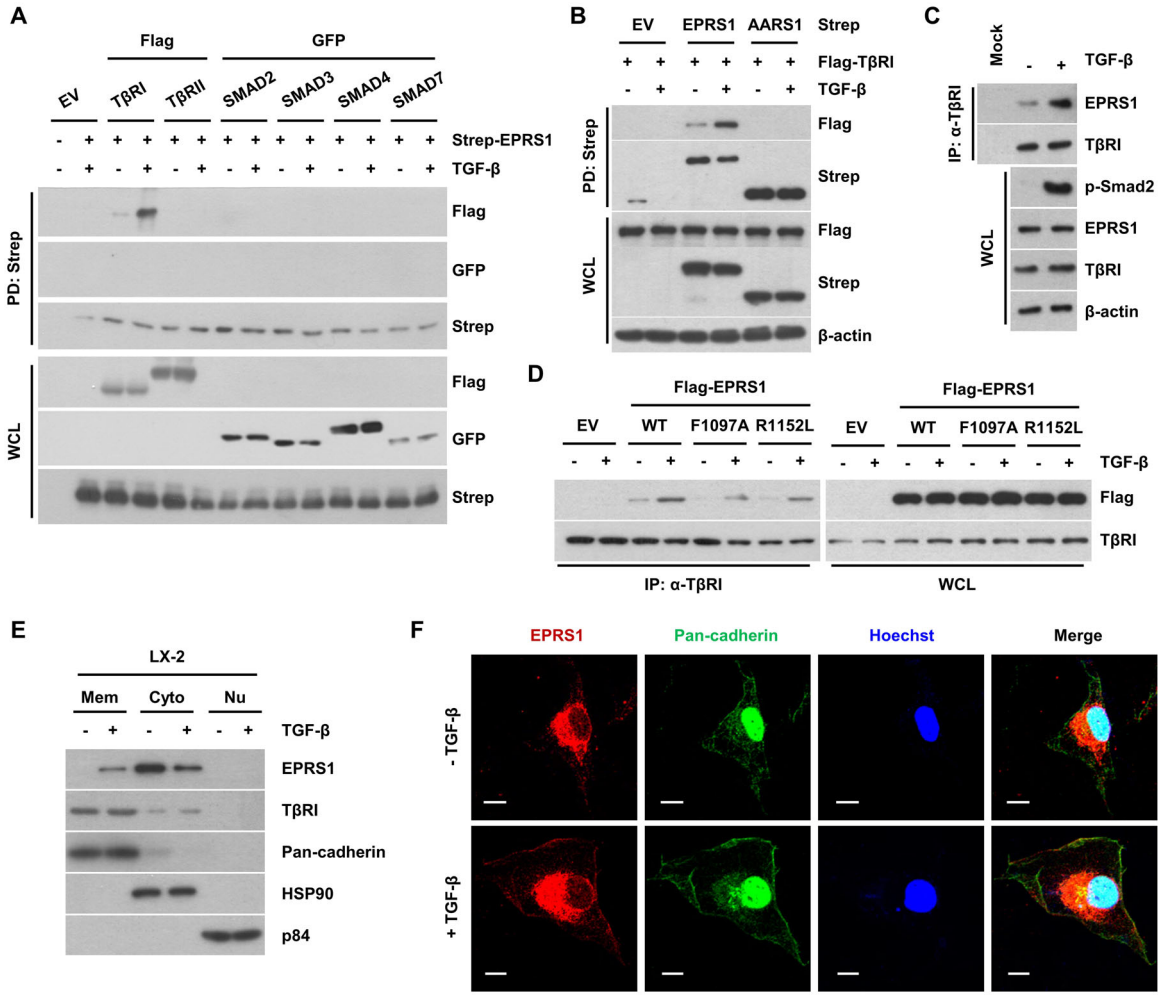


**FIG 2** TGF-β-dependent interaction between EPRS1 and TβRI. (A) HEK293T cells were transfected with the indicated plasmids and incubated in the absence or presence of TGF-β for 2 h. Cell lysates were pulled down with MagStrep beads and coprecipitated proteins were determined by immunoblot assay. PD, pull-down; WCL, whole cell lysates. (B) HEK293T cells were transfected with the indicated plasmids and incubated in the absence or presence of TGF-β for 2 h. Cell lysates were pulled down with MagStrep beads and coprecipitated proteins were determined using immunoblot assay. PD, pull-down; WCL, whole cell lysates. (C) LX-2 cells were treated with TGF-β for 2 h. The interaction between EPRS1 and TβRI was determined by immunoblot assay. Mock, IgG control. (D) LX-2 cells were incubated in the presence of doxycycline to induce stable expression of the indicated proteins. The cells were incubated in the absence or presence of TGF-β for 2 h. The interaction between EPRS1 and TβRI was determined by immunoblot assay. IP, immunoprecipitation. (E) LX-2 cells were incubated in the absence or presence of TGF-β for 2 h and subcellular compartment was separated to membrane, cytosol and nucleus fractions. Subcellular localization of the indicated proteins was determined by immunoblot assay. Mem, membrane fraction; Cyto, cytosolic fraction; Nu, nuclear fraction. (F) LX-2 cells were starved of serum for 17 h and then incubated in the presence or absence of TGF-β for 20 min. Cells were incubated with anti-EPRS1 and anti-pan-cadherin antibodies and then visualized with Alexa-647- and Alexa-488-conjugated secondary antibodies, respectively. Hoechst was used to stain nucleus. Scale bar, 10 μm.

We additionally monitored subdomains of PARS1 and TβRI that are responsible for the interaction through pull-down assays. Results showed that TβRI interacted with anti-codon-binding domain (ABD) of PARS1 (Fig. 3B) and PARS1 bound to glycine-serine rich (GS) domain of TβRI (Fig. 3C). The interaction between PARS1 and TβRI was found to be a direct interaction through in vitro pull-down and microscale thermophoresis (MST) assays (Fig. 3D and E).

**TAK1 phosphorylates EPRS1 in response to TGF-β.** Next, we assessed posttranslational modifications of EPRS1 in the absence or presence of TGF-β. EPRS1 was prominently phosphorylated at threonine and weakly at serine residues in response to TGF-β (Fig. 4A). To identify the kinase phosphorylating EPRS1 in response to TGF-β stimulation, we prepared inhibitors of kinases that are activated in the presence of TGF-β. In the kinase inhibitor screening assay, the phosphorylation of EPRS1 at serine and threonine residues was decreased following treatment with 5Z-7-oxozeaenol, an inhibitor of

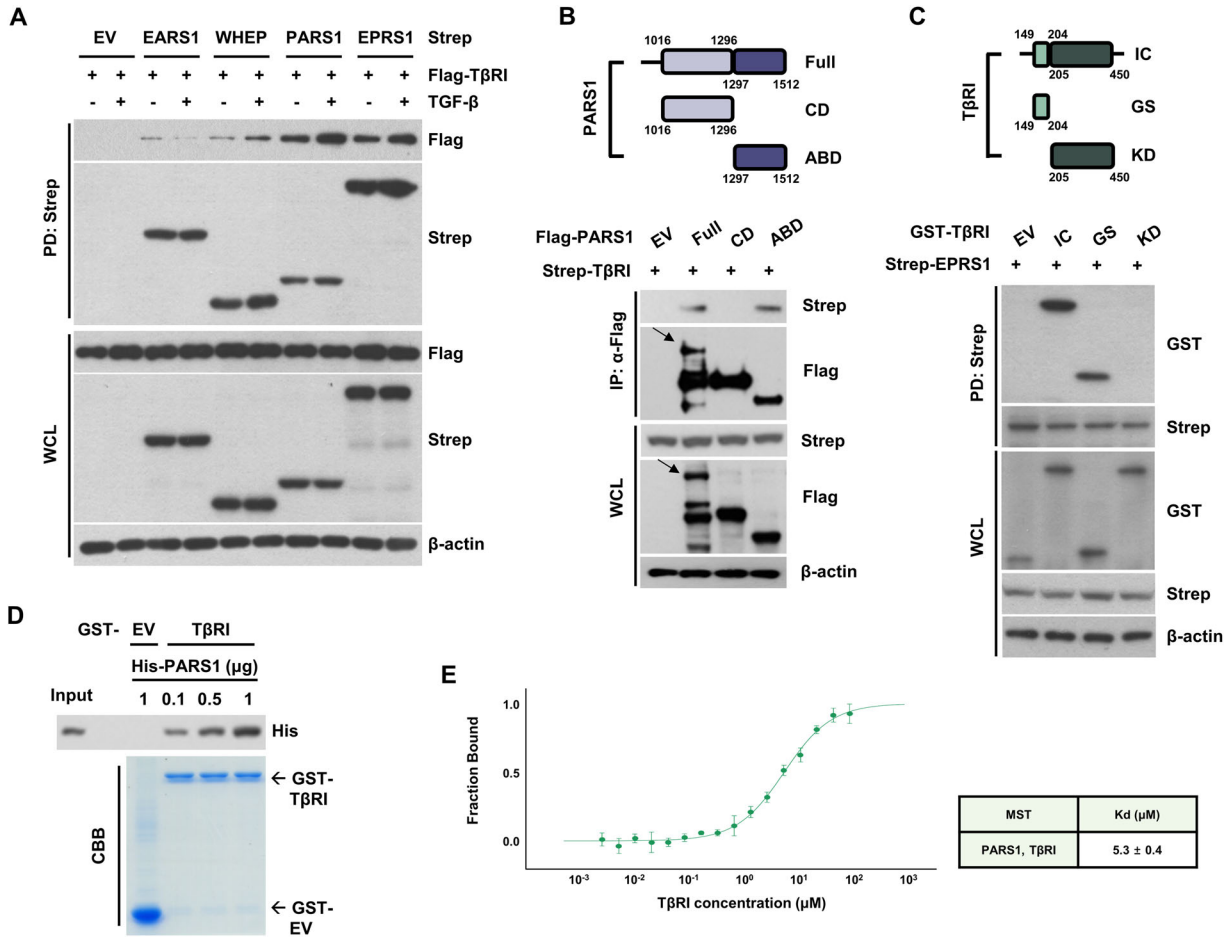


**FIG 3** Determination of interacting domains of EPRS1 and TβRI. (A) HEK293T cells were transfected with the indicated plasmids and incubated in the absence or presence of TGF-β for 2 h. The interaction between TβRI and EPRS1 fragments were determined through pull-down assay. (B) HEK293T cells were co-transfected with Strep-TβRI and Flag-PARS1 fragments. Cell lysates were immunoprecipitated with anti-flag M2 affinity gel and coprecipitated TβRI was determined by immunoblot assay. CD, catalytic domain; ABD, anticodon-binding domain. (C) HEK293T cells were transfected with Strep-EPRS1 and cell lysates were pulled down with MagStrep beads. *In vitro* purified TβRI fragments were incubated with the pulled down Strep-EPRS1 and coprecipitated TβRI fragments were determined by immunoblot assay. IC, intracellular; GS, glycine-serine rich domain; KD, kinase domain. (D) *In vitro* pull-down assay using His-PARS1 and GST-TβRI. Dose-dependent interaction between PARS1 and TβRI was determined using immunoblot assay. CBB, Coomassie brilliant blue staining. (E) *In vitro* interaction between PARS1 and TβRI was determined through microscale thermophoresis (MST) assay. Dissociation constant between PARS1 and TβRI was listed in the table.

TGF-β-activated kinase 1 (TAK1) (Fig. 4B).[32] 5Z-7-Oxozeaenol-dependent inhibition of EPRS1 phosphorylation was also confirmed by immunoprecipitation of the endogenous EPRS1 (Fig. 4C). To rule out the nonspecific inhibition of other kinases by 5Z-7-oxozeaenol, we monitored EPRS1 phosphorylation in cells transfected with siRNAs targeting *TAK1*. Knockdown of TAK1 decreased EPRS1 phosphorylation, further validating TAK1-dependent phosphorylation of EPRS1 (Fig. 4D). We then monitored the association of EPRS1 with the MSC in the absence or presence of TGF-β, and evaluated the effect of EPRS1 phosphorylation on its association with the MSC. Following TGF-β treatment, EPRS1 was dissociated from the MSC, while one of the other MSC components, LARS1, remained within the complex. The TGF-β-induced dissociation of EPRS1 was partially inhibited in the presence of 5Z-7-oxozeaenol (Fig. 4E). In contrast, TAK1 suppression reduced the TGF-β-dependent interaction between EPRS1 and TβRI (Fig. 4F). These results suggest that EPRS1 is phosphorylated by TAK1 in the presence of TGF-β which leads to the dissociation of EPRS1 from the MSC and association to TβRI.

To study TAK1-mediated EPRS1 phosphorylation more specifically, we examined direct phosphorylation of EPRS1 by TAK1. Through an *in vitro* kinase assay using radioactive isotope, we found that EPRS1 that is pulled down from 293 T cell lysates was

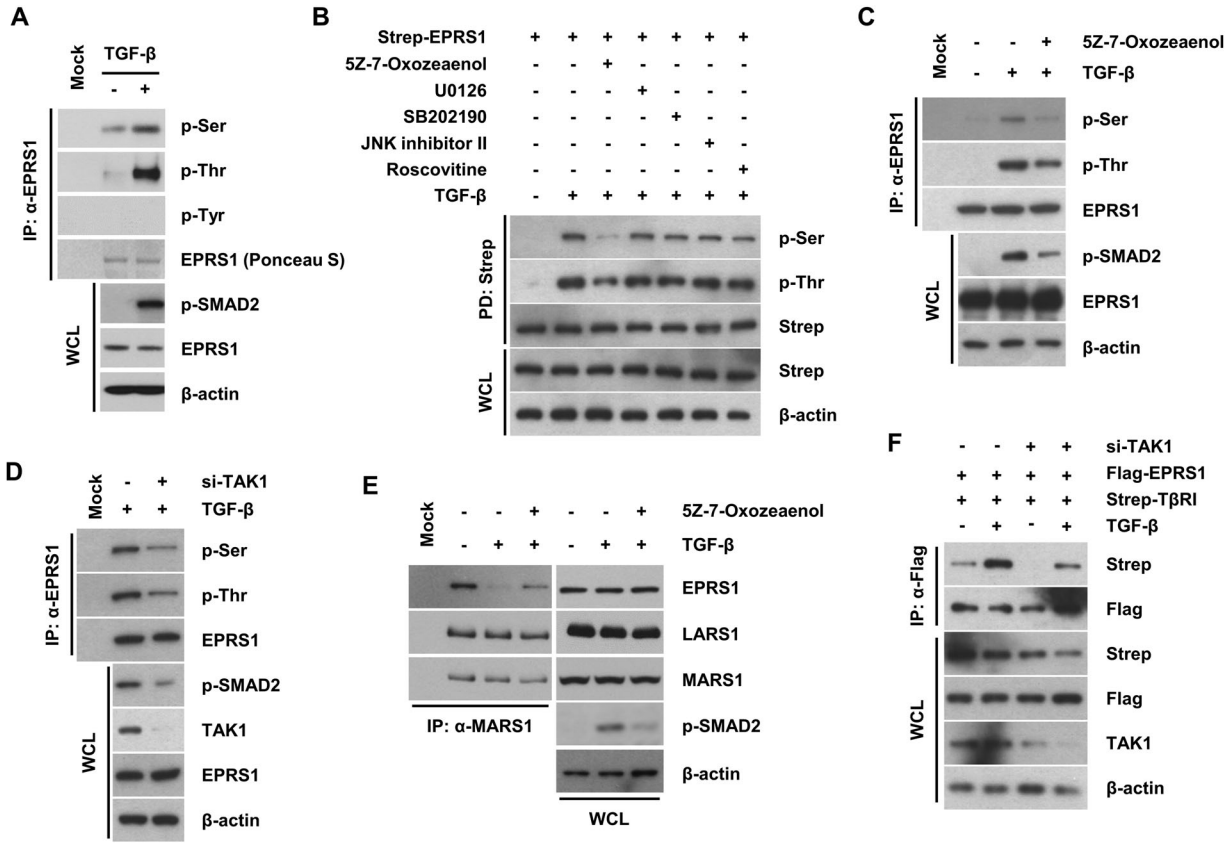


**FIG 4** TGF-β-dependent phosphorylation of EPRS1 by TAK1. (A) LX-2 cells were starved of serum for 12 h and then incubated in the presence of TGF-β for 20 min. Cell lysates were prepared and immunoprecipitated with anti-EPRS1 antibody. The levels of phosphoserine, phosphothreonine, and phosphotyrosine were determined by immunoblot assay. IP, immunoprecipitation; WCL, whole cell lysates. (B) HEK293T cells were transfected with Strep-EPRS1 and incubated with the indicated compounds for 4 h. TGF-β was supplemented for the last 20 min in groups designated as TGF-β positive. Cells lysates were prepared and pulled down with MagStrep beads. The levels of phosphoserine and phosphothreonine were determined by immunoblot assay. 5Z-7-oxozeaenol, TAK1 inhibitor; U0126, ERK inhibitor; SB202190, p38 MAPK inhibitor, JNK inhibitor II, JNK inhibitor; roscovitine, CDKs inhibitor. (C) LX-2 cells were incubated with 5Z-7-oxozeaenol for 4 h and TGF-β was supplemented for the last 20 min in groups designated as TGF-β positive. Cell lysates were prepared and immunoprecipitated with anti-EPRS1 antibody. The levels of phosphoserine and phosphothreonine were determined by immunoblot assay. (D) LX-2 cells were transfected with siRNAs targeting *TAK1* and treated with TGF-β for 20 min. Cell lysates were prepared and immunoprecipitated with anti-EPRS1 antibody. The levels of phosphoserine and phosphothreonine were determined by immunoblot assay. (E) LX-2 cells were incubated with 5Z-7-oxozeaenol for 4 h and TGF-β was supplemented for the last 20 min in groups designated as TGF-β positive. Cell lysates were immunoprecipitated with anti-MARS1 antibody and coprecipitation of EPRS1 was determined by immunoblot assay. (F) HEK293T cells were transfected with the indicated plasmids and siRNAs. After the cells were incubated in the absence or presence of TGF-β for 2 h, the interaction between EPRS1 and TβRI was monitored through immunoprecipitation assay.

phosphorylated by TAK1-TAK1 binding protein 1 (TAB1) fusion protein, which mimics the active form of TAK1 (Fig. 5A).[33] To rule out the possible involvement of EPRS1-interacting proteins in the phosphorylation reaction, and provide evidence for the direct phosphorylation of EPRS1 by TAK1, we tried to conduct *in vitro* kinase assay by using purified EPRS1 protein. Since EPRS1 was insoluble in a bacterial expression system, we used purified EARS1 (amino acid residues 194–709) and WHEP + PARS1 (amino acid residues 747–1512) proteins (Fig. 5B)[34] and found that EARS1 domain was directly phosphorylated by TAK1-TAB1 fusion protein (Fig. 5C). Since EPRS1 was phosphorylated at both threonine and serine residues upon stimulation with TGF-β (Fig. 4A and C), we further tested *in vitro* phosphorylation of 293 T cell-derived full-length EPRS1 by TAK1-TAB1. Full-length EPRS1 was also phosphorylated at threonine but not serine residues (Fig. 5D). In addition, TAK1-directed phosphorylation of EPRS1 did not enhance the interaction between EPRS1 and TβRI (Fig. 5E). These results suggest that TGF-β-induced phosphorylation of EPRS1 at threonine residue is mediated by TAK1 directly, but that of EPRS1 at serine residue might be mediated by TAK1 indirectly.

**EPRS1 controls stability of TβRI.** Based on our observation that EPRS1 modulates SMAD2 phosphorylation and interacts with TβRI, we postulated that EPRS1 would

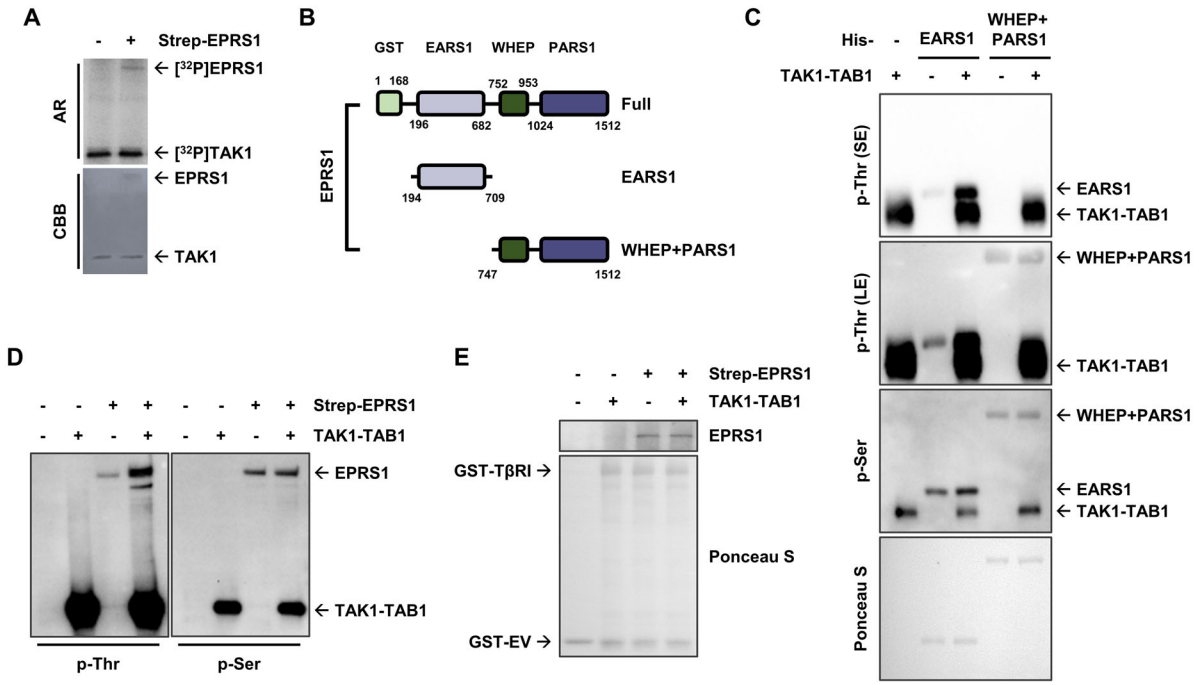


**FIG 5** Effect of EPRS1 phosphorylation on the interaction with TβRI. (A) HEK293T cells were transfected with empty vector or Strep-EPRS1 and pulled down with MagStrep beads. The samples were incubated with TAK1-TAB1 fusion protein for *in vitro* phosphorylation in the presence of [$\gamma$-$^{32}$P]ATP. Phosphorylation of proteins were detected through autoradiography (AR). CBB, Coomassie brilliant blue staining. (B) Schematic representation of EPRS1 domains. (C) EARS1 and WHEP + PARS1 proteins were purified in bacterial expression systems and incubated with TAK1-TAB1 fusion protein for *in vitro* phosphorylation. The levels of phosphoserine and phosphothreonine were determined by immunoblot assay. SE, short exposure; LE, long exposure. (D and E) Strep-EPRS1 proteins were prepared by transfection to HEK293T cells, pulled down with strep beads, and elution. The eluted Strep-EPRS1 proteins were incubated in the presence or absence of TAK1-TAB1 fusion protein for *in vitro* phosphorylation and then incubated with GST-EV or GST-TβRI for pull-down assay. Phosphorylation of EPRS1 was determined by phosphothreonine- and phosphoserine-specific antibodies (D). Coprecipitated EPRS1 was detected by immunoblot assay (E).

regulate the TGF-β signaling pathway by modulating TβRI stability since TβRI stability control is the major regulatory point for the TGF-β signaling pathway.[8,9] We monitored the stability of TβRI in EPRS1 overexpressing and EPRS1 knockdown cells. When cells were treated with cycloheximide (CHX) to inhibit de novo protein synthesis, thereby the cellular protein levels were determined only by their half-lives, TβRI protein degradation was slower in cells with the ectopic expression of EPRS1, whereas it was faster in EPRS1 knockdown cells (Fig. 6A, B and C). In addition, overexpression of EPRS1 decreased TβRI ubiquitination (Fig. 6D and E), whereas EPRS1 knockdown increased the ubiquitination of TβRI (Fig. 6F and G). These results suggest that EPRS1 inhibits the ubiquitination of TβRI, thereby improving its stability.

Since the stability of TβRI is regulated by SMAD7 during TGF-β-initiated pathway activation,[9] we evaluated the interaction between EPRS1, TβRI, and SMAD7. TβRI and SMAD7 interaction was decreased in cells overexpressing EPRS1 (Fig. 7A). Specifically, the PARS1 domain of EPRS1 was required for the dissociation of TβRI from SMAD7 (Fig. 7B). In addition, the levels of TβRI ubiquitination were negatively correlated with EPRS1 protein levels (Fig. 7C), suggesting that EPRS1 abrogates the interaction between TβRI and SMAD7, resulting in the inhibition of SMAD7-mediated E3 ligase recruitment and subsequent TβRI ubiquitination.

Next, we evaluated the role of EPRS1 in regulating the interaction between SMAD2/3, SMAD7, and TβRI. TβRI was pulled down in lysates of cells with EPRS1 overexpression or knockdown, and the levels of coprecipitated SMAD2/3 and SMAD7 were analyzed. EPRS1 overexpression enhanced the interaction between SMAD2/3 and TβRI while decreased the interaction of SMAD7 with TβRI (Fig. 7D). In contrast, EPRS1 knockdown decreased the interaction between SMAD2/3 and TβRI while increased the

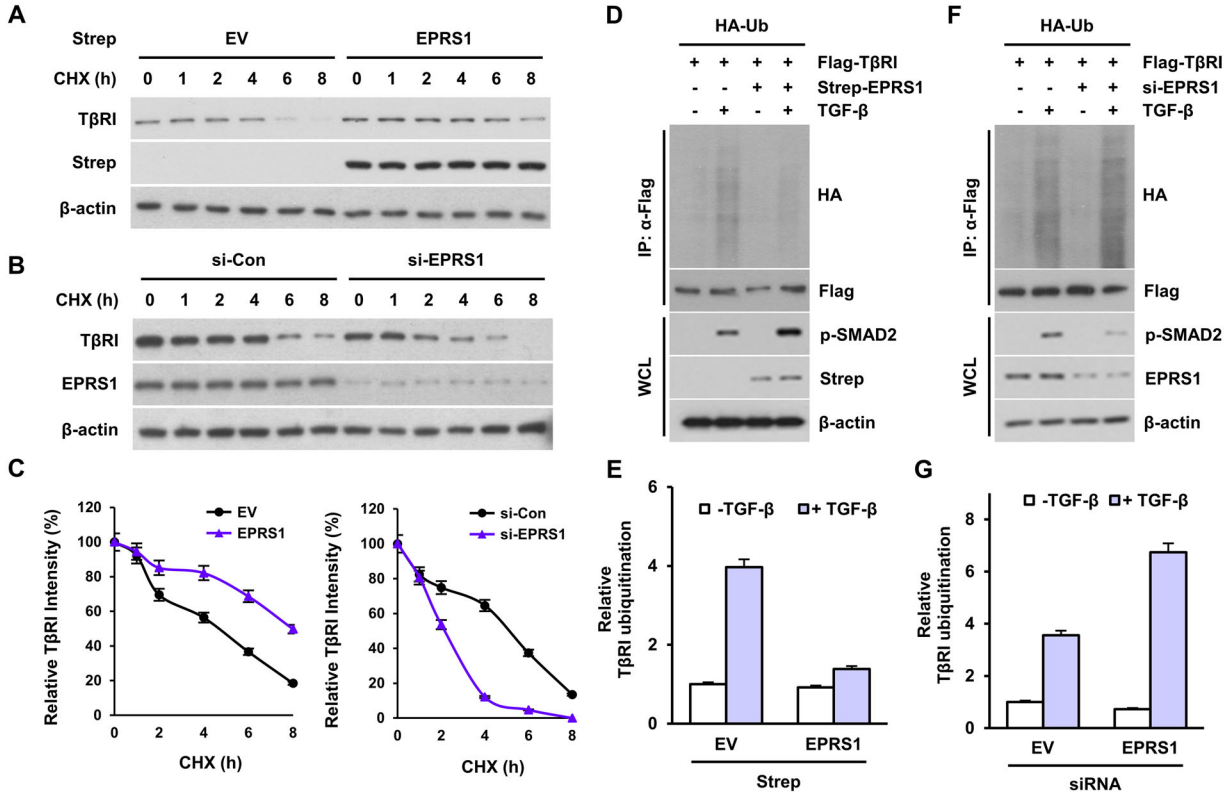


**FIG 6** Effect of EPRS1 on the stability of TβRI. (A) LX-2 cells were transfected with plasmids expressing empty vector (EV) or EPRS1 and incubated in the presence of cycloheximide (CHX) for the indicated time. The level of TβRI was determined by immunoblot assay. (B) LX-2 cells were transfected with non-targeting siRNAs (si-Con) or siRNAs targeting *EPRS1* (si-*EPRS1*) and incubated in the presence of CHX for the indicated time. The level of TβRI was determined by immunoblot assay. (C) Relative level of TβRI was quantified based on (A) (left) and (B) (right). Band intensity of each time point was normalized relative to that of initial time point ($t = 0$). (D to G) LX-2 cells were transfected with the indicated plasmids and siRNAs and then, incubated in the absence or presence of TGF-β for 6 h. MG132 was additionally supplemented to cells for the last 4 h. Cell lysates were immunoprecipitated with anti-Flag M2 gel and ubiquitination levels of TβRI were determined by immunoblot.

interaction of SMAD7 with TβRI (Fig. 7E). In addition, the interaction between SMAD2 and SMAD4 was positively regulated by EPRS1 (Fig. 7F and G), implying the role of EPRS1 as a positive mediator of TGF-β pathway activation. These results imply that EPRS1 modulates recruitment of SMAD proteins to TβRI.

**HF modulate the interaction between EPRS1 and TβRI.** Since the potential involvement of EPRS1 in the TGF-β pathway was first suggested by studies showing that HF reduces R-SMADs phosphorylation, we investigated the effect of HF on the interaction between EPRS1 and TβRI. Using the *in vitro* pull-down assay, we observed that HF, but not borrelidin, a catalytic inhibitor of threonyl-tRNA synthetase 1 (TARS1),[35,36] inhibited the binding of EPRS1 to TβRI (Fig. 8A). Moreover, cells incubated with HF showed decreased levels of TβRI, collagen I, α-SMA, and phospho-SMAD2 (Fig. 8B). In addition, HF reduced the contractility of HSCs (Fig. 8C), implying that HF modulates the TGF-β pathway by disrupting the interaction between EPRS1 and TβRI, leading to the subsequent degradation of TβRI.

Overall, we showed a noncatalytic role of EPRS1 in regulating the TGF-β signaling pathway and elucidated the underlying molecular mechanism. In the presence of TGF-β, EPRS1 is phosphorylated by TAK1 leading to its dissociation from the MSC. Phosphorylated EPRS1 then interacts with TβRI and this interaction increases the association of TβRI and SMAD2/3, while decreases the association between TβRI and SMAD7. Consequently, SMAD7-mediated recruitment of the E3 ligase and subsequent TβRI ubiquitination were reduced. As a result, EPRS1 promotes activation of the TGF-β pathway by preventing TβRI degradation. HF disrupts the interaction between EPRS1 and TβRI, and consequently reduce TβRI levels, suggesting dual functions (catalytic and noncatalytic) of EPRS1 and the corresponding dual inhibitory activities of HF (Fig. 8D).

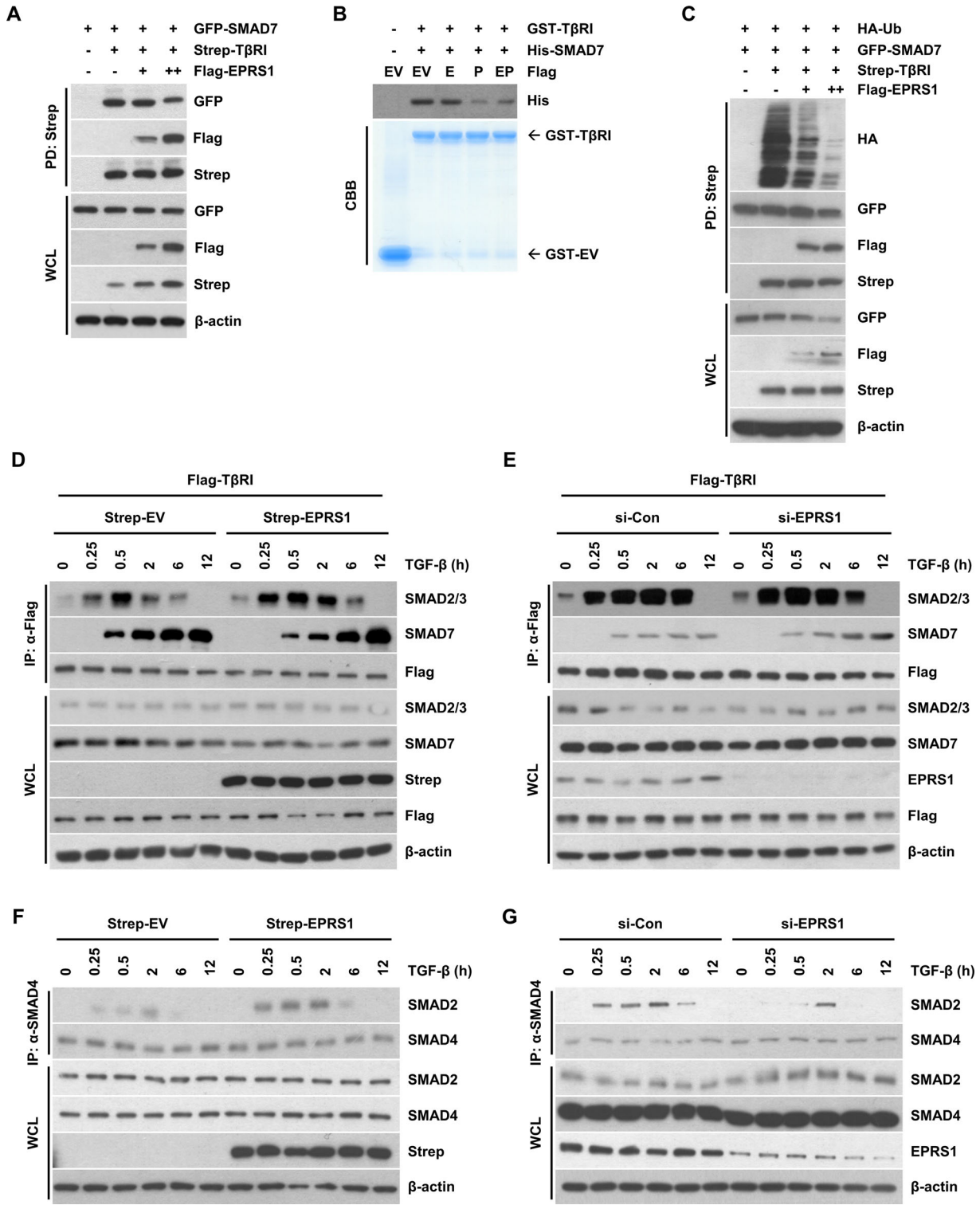


**FIG 7** Effect of EPRS1 on the SMAD7-dependent ubiquitination of TβRI. (A) HEK293T cells were transfected with the indicated plasmids, followed by TGF-β stimulation for 6 h. Interaction of TβRI with SMAD7 or EPRS1 was determined by immunoblot assay. PD, pulldown; WCL, whole cell lysates. (B) HEK293T cells were transfected with each of Flag-EV, EARS1, PARS1, or EPRS1 and cell lysates were immunoprecipitated with anti-Flag M2 gel. After Flag-EV, EARS1, PARS1, or EPRS1 proteins were obtained through elution with Flag peptide, *in vitro* pull-down assay of GST-TβRI with His-SMAD7 was conducted in the presence of the eluted proteins. The interaction between TβRI and SMAD7 was determined by immunoblot assay. CBB, Coomassie brilliant blue staining. (C) HEK293T cells were transfected with the indicated plasmids and incubated in the presence of MG132 for 4 h. Level of TβRI ubiquitination was determined by immunoblot assay. (D and E) HEK293T cells were transfected with the indicated plasmids and siRNAs, and incubated in the presence of TGF-β for the indicated time. The interaction of TβRI with SMAD2/3 or SMAD7 was determined by immunoblot assay. IP, immunoprecipitation. (F and G) HEK293T cells were transfected with the indicated plasmids or siRNAs, and treated with TGF-β for the indicated time. Interaction between SMAD2 and SMAD4 was determined by immunoprecipitation followed by immunoblot assay. IP, immunoprecipitation; WCL, whole cell lysates.

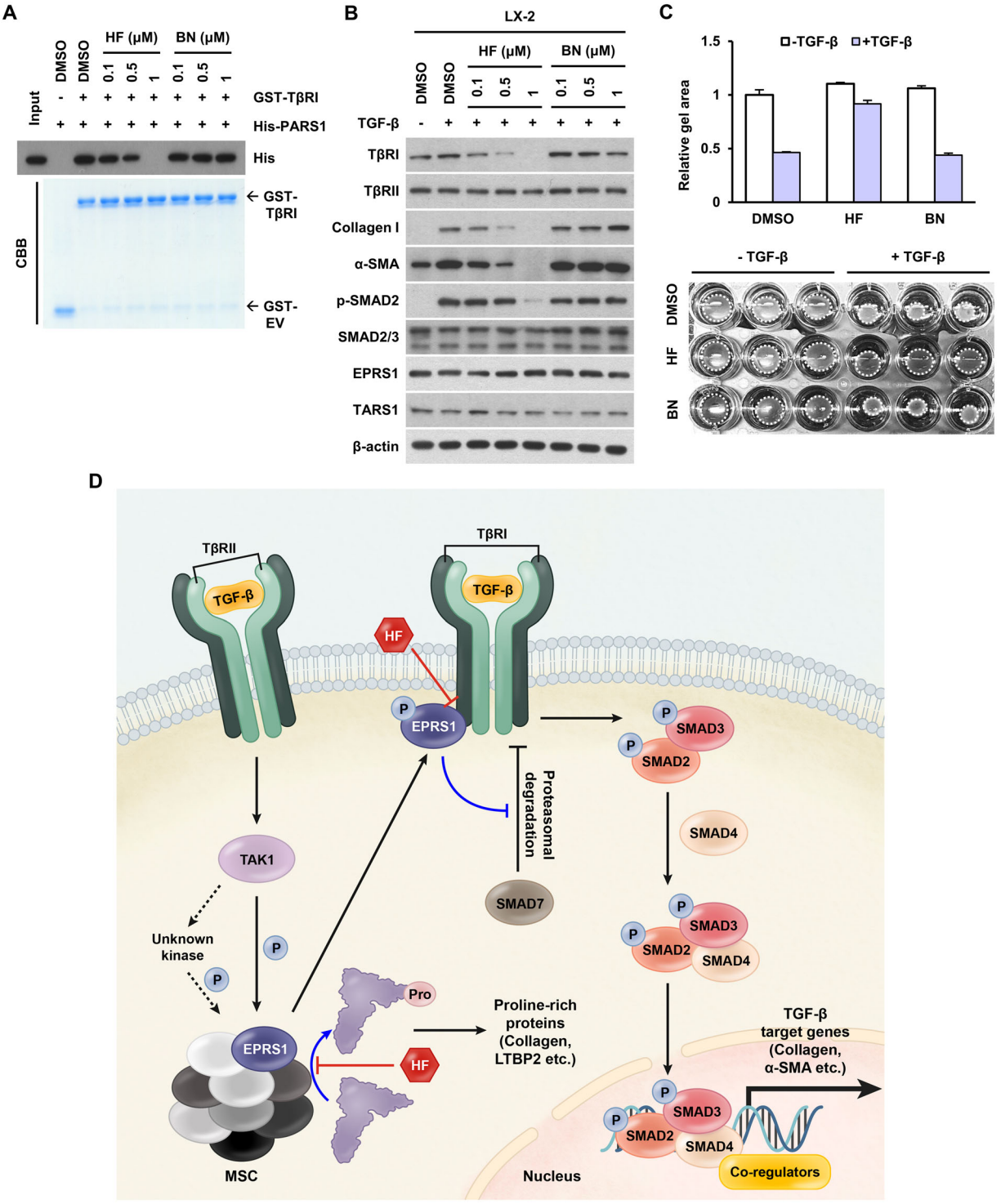


**FIG 8** Effect of HF on the interaction between EPRS1 and TβRI. (A) *In vitro* pulldown assay using His-PARS1 and GST-TβRI. Coprecipitated level of His-PARS1 protein was determined by immunoblot assay. BN, borrelidin. CBB, Coomassie brilliant blue staining. (B) LX-2 cells were incubated with TGF-β and the indicated compounds for 6 h. Levels of the indicated proteins involved in the TGF-β signaling pathway were determined by immunoblot assay. (C) LX-2 cells were mixed with collagen and incubated with HF or BN in the absence or presence of TGF-β. Relative collagen gel size was determined based on the white dotted circle (lower). Relative gel area was displayed as bar graph (upper) ($n = 3$, mean ± SEM). Schematic representation about EPRS1-mediated control of TGF-β-induced fibrosis and its inhibition by HF. The roles of EPRS1 are presented as blue arrows and those of HF are presented as red.

## DISCUSSION

Hepatic fibrosis is a chronic and progressive disease characterized by excessive accumulation of the ECM proteins, especially collagen.[1] Although early phase of liver fibrosis

is known to be a reversible state, the detailed mechanism to reverse hepatic fibrosis is not fully understood.[3] Accordingly, effective ways to treat hepatic fibrosis are still under investigation despite various approaches.[37] As an approach to relieve liver fibrosis, reducing collagen levels has been of interest. Since HF was known to decrease collagen levels,[22] there have been some efforts to control hepatic fibrosis using HF.[37–39]

Although it is known that HF ameliorates fibrosis by reducing pro-tRNA levels and decreasing SMAD2/3 phosphorylation, the exact mechanism by which HF regulates TGF-β-mediated SMAD2/3 phosphorylation has not been fully understood. To understand this mechanism, we postulated that EPRS1, a target protein of HF, would be involved in regulating the TGF-β pathway. We investigated the role of EPRS1 using the catalytic activity-defective EPRS1 mutants, since collagen production during fibrosis is determined by both EPRS1 catalytic activity and TGF-β pathway activation. LX-2 cells, a hepatic stellate cell line, expressing EPRS1 WT or mutants showed that both catalytic and noncatalytic activities of EPRS1 are required for collagen production (Fig. 1H), suggesting dual functions of EPRS1 in controlling fibrosis (Fig. 8D). Considering the significance of the TGF-β pathway in the development of hepatic fibrosis, both functions of EPRS1 mediating the TGF-β pathway as well as regulating the synthesis of proline-rich proteins such as collagen may be involved in pathogenesis of liver fibrosis and be applied as a potential target point.

Although we observed TAK1-mediated phosphorylation of EPRS1 and its subsequent dissociation from the MSC (Fig. 4), the role of TAK1 in development of hepatic fibrosis is quite complex. Mice with hepatocyte-specific knockout of TAK1 develop spontaneous liver fibrosis along with HSC activation.[40] In contrast, HSCs with TAK1 knockdown shows decreased α-SMA levels.[41] Considering the opposing roles of TAK1 in hepatocytes and HSCs, cell line-specific phosphorylation of EPRS1 and its role in the development of fibrosis should be further investigated.

Despite our effort to investigate TGF-β-dependent phosphorylation of EPRS1, it remains unclear which kinase, including TAK1, phosphorylates EPRS1, which residues are phosphorylated by the kinases, and what the exact role of the phosphorylation is. Although we observed TGF-β-dependent phosphorylation of EPRS1 at serine and threonine residues (Fig. 4A and C), it seems that TAK1 directly mediates only threonine phosphorylation (Fig. 5C and D), implying the existence of another kinase. Considering that chemical and biological suppression of TAK1 decreases EPRS1 phosphorylation at both serine and threonine residues (Fig. 4C and D), TAK1 may mediate serine phosphorylation of EPRS1 in an indirect manner through an unknown kinase (Fig. 8D). In addition, the exact role of each phosphorylation residues should be further investigated in regulating the interaction of EPRS1 with the MSC and TβRI. At this moment, TAK1-mediated threonine phosphorylation seems to be not involved in the binding with TβRI (Fig. 5E), which makes sense considering the TAK1-mediated phosphorylation domain (EARS1) (Fig. 5C) and the TβRI-interacting domain (PARS1) (Fig. 3A).

The interaction between EPRS1 and TβRI was found to be quite specific among the proteins involved in the canonical TGF-β pathway (Fig. 2A). Considering that EPRS1 helps in maintaining the TβRI-SMAD2/3 complex and interferes with the formation of the TβRI-SMAD7 complex (Fig. 7D and E), it might be possible that EPRS1 induces conformational changes in TβRI to alter its affinity toward SMAD2/3 and SMAD7. Since SMAD2/3 and SMAD7 bind to TβRI via the same domain, MH2 domain, their interaction with TβRI is supposed to be competitive.[42,43] Therefore, the binding of EPRS1 to TβRI may induce conformational change of TβRI to increase affinity to SMAD2/3 and to decrease affinity to SMAD7. Further structural analysis of the TβRI-EPRS1 complex can provide clues to conformational changes in TβRI and the molecular mechanism regulating its affinity.

In previous reports demonstrating the function of EPRS1 in TGF-β-induced STAT6 activation for the ECM proteins production,[28,29] EPRS1 binding to TβRI was reduced upon STAT6 knockdown in A549 and LX-2 cells, suggesting that STAT6 may help the complex formation of EPRS1 and TβRI. Although the exact architectural information of the complex consisting of EPRS1, JAKs, STATs and SMADs is not available, further studies on

interacting domain mapping of the complex may provide clues. In addition, considering the cross-talk between SMAD1 and STAT3 through common coactivators such as p300/CBP (CREB binding protein),[44] the significance of EPRS1 regulation to both STAT and SMAD signaling pathways may be explored for the effective transcriptional control of the target genes.

When monitoring the effect of HF, HF disrupts the interaction between TβRI and EPRS1, and reduces protein levels of TβRI, collagen I, α-SMA, and phospho-SMAD2 in LX-2 cell line (Fig. 8A and B). Considering possible applicability of HF in various fibrotic diseases, unveiling the novel functions of its target protein EPRS1 in controlling the fibrotic TGF-β pathway will provide insight to develop new compounds. Since the contribution of HF activities inhibiting tRNA prolylation and SMAD2/3 phosphorylation to drug efficacy and adverse effect remains unclear, further studies on functional significance of each role of EPRS1 in fibrogenesis and the inhibitory effect of HF will suggest the direction to improve EPRS1-targeting compound against fibrosis.

Altogether, we revealed a novel function of EPRS1 in controlling the TGF-β pathway via the interaction with TβRI and its association with HSCs activation and possible fibrogenesis. In addition, we showed the inhibitory effects of HF on the novel function of EPRS1, suggesting potential use of HF to hepatic fibrosis.

## MATERIALS AND METHODS

**Cell culture and transfection.** HEK293T cells were obtained from American Type Culture Collection (ATCC). LX-2 cells were obtained from Millipore (SCC064). HEK293T and LX-2 cells cultures in Dulbecco's Modified Eagle's Medium (DMEM) (Cytiva, SH30243.01) supplemented with 10% fetal bovine serum (FBS) (Cytiva, SH30084.03) and 1% penicillin-streptomycin (Cytiva, SV30010), and grown in 5% $CO_2$ at 37 °C. The cells were transfected with plasmid DNAs or siRNAs using TurboFect (Thermo Fisher Scientific, R0534) following the manufacturer's instructions.

**TABLE 1** Plasmids used in this study

| Name of plasmid and description | Source |
|---|---|
| pLVX-tetOne-puro | Clontech, 631849 |
| pEXPR-IBA-103 | IBA, 2-3503-000 |
| pLVX-tetOne-puro-flag-EPRS1 | This study |
| pLVX-tetOne-puro-flag-EPRS1 F1097A | This study |
| pLVX-tetOne-puro-flag-EPRS1 R11152L | This study |
| pET28a-PARS1 (1001-1512) | 26 |
| pET28a-PARS1 (1001-1512 AA of EPRS1) F1097A | 26 |
| pET28a-PARS1 (1001-1512 AA of EPRS1) R1152L | 26 |
| pET28a-EARS1 (194-709) | This study |
| pET28a-(WHEP + PARS1) (747-1512) | This study |
| pEXPR-IBA-103-EPRS1 | This study |
| pEXPR-IBA-103-AARS1 | This study |
| Flag-TβRI | This study |
| Flag-TβRII | This study |
| GFP-SMAD2 | This study |
| GFP-SMAD3 | This study |
| GFP-SMAD4 | This study |
| GFP-SMAD7 | This study |
| pCMV6-AC-MYCDDK-EPRS1 | Origene, RC217559 |
| pCMV6-AC-MYCDDK-EPRS1 F1097A | This study |
| pCMV6-AC-MYCDDK-EPRS1 R1152L | This study |
| pEXPR-IBA-103-TβRI | This study |
| pEXPR-IBA-103-EARS1 | This study |
| pEXPR-IBA-103-WHEP | This study |
| pEXPR-IBA-103-PARS1 | This study |
| pGEX-4T1-TβRI | This study |
| HA-Ub | This study |
| Flag-PARS1 CD | This study |
| Flag-PARS1 ABD | This study |
| pGEX-4T1-TβRI intracellular | This study |
| pGEX-4T1-TβRI GS | This study |
| pGEX-4T1-TβRI KD | This study |

**TABLE 2** siRNAs used in this study

| siRNA name | Source | Catalog number |
|---|---|---|
| si-Con | Thermo Fisher Scientific | 12935400 |
| si-EPRS1 | Thermo Fisher Scientific | HSS103321 |
| si-TAK1 | Thermo Fisher Scientific | HSS110464 |

**TABLE 3** Antibodies used in this study

| Name of antibody | Source | Catalog number |
|---|---|---|
| p-SMAD2 | Cell Signaling Technology | 3108 |
| SMAD2/3 | Cell Signaling Technology | 8685 |
| α-SMA | Merck Millipore | CBL171-I |
| Collagen I | DSBH | SP1.D8 |
| Strep-HRP | IBA life sciences | 2-1509-001 |
| β-Actin | Sigma-Aldrich | A1978 |
| EPRS1 | Neomics | NMS-01-0004 |
| Flag | Sigma-Aldrich | F3165 |
| Phosphoserine | Abcam | ab9332 |
| Phosphothreonine | Cell Signaling Technology | 9381 |
| Phosphotyrosine | Millipore | 05-321 |
| TAK1 | Cell Signaling Technology | 5206 |
| LARS1 | Bethyl Laboratories | A304-315A |
| MARS1 | Abcam | ab50793 |
| GFP | Santa Cruz Biotechnology | sc-9996 |
| TβRI | Santa Cruz Biotechnology | sc-9048 |
| Pan-cadherin | Santa Cruz Biotechnology | sc-515872 |
| HSP90 | Santa Cruz Biotechnology | sc-7947 |
| His | Santa Cruz Biotechnology | sc-8036 |
| HA | Santa Cruz Biotechnology | sc-7392 |
| SMAD7 | Santa Cruz Biotechnology | sc-365846 |
| SMAD4 | Cell Signaling Technology | 46535 |
| TβRII | Santa Cruz Biotechnology | sc-220 |
| Mouse IgG (H + L) secondary antibody (HRP) | Thermo Fisher Scientific | 31430 |
| Rabbit IgG (H + L) secondary antibody (HRP) | Thermo Fisher Scientific | 31460 |
| Rabbit TrueBlot®: Anti-rabbit IgG HRP | Rockland | 18-8816-31 |
| Mouse TrueBlot® ULTRA: Anti-mouse Ig HRP | Rockland | 18-8817-30 |
| Goat anti-rabbit IgG (H + L) Cross-adsorbed Secondary Antibody, Alexa Fluor™ 647 | Thermo Fisher Scientific | A21244 |
| Chicken anti-mouse IgG (H + L) Cross-adsorbed Secondary Antibody, Alexa Fluor™ 488 | Thermo Fisher Scientific | A21200 |

**Plasmids and antibodies (Tables 1–4).**

**Lentiviral transduction and stable cell line establishment.** Flag-EPRS1 WT, F1097A, R1152L were subcloned to pLVX-TetOne™-Puro vector (Clontech, 631849). Lentiviruses were produced by Lenti-X 293 T cells (Clontech, 632180) using Lenti-X Tet-On advanced inducible expression system (Clontech, 632162) following the manufacturer's instructions. Viruses in supernatant of Lenti-X 293 T were collected 48 h after transfection. Then, LX-2 cells were infected with the lentiviral supernatants in the presence of 8 μg/mL of polybrene. After incubated with the supernatant for 24 h, the infected cells were selected using puromycin (1 μg/mL) for 2 weeks. To induce protein expression, cells were incubated in the presence of doxycycline (2 μg/mL) for 96 h.

**In vitro prolylation assay.** To determine the prolylation activities of PARS1 WT, F1097A and R1152L, the reaction buffer (20 mM Tris-HCl (pH 7.5), 6 mM MgAc, 0.5 mM DTT, 5 mM ATP, 5 mg/mL yeast total tRNA, 1 μM [$^3$H]proline (81.4 Ci/mmol)) was prewarmed at 37 °C. The enzymatic reaction was initiated by the addition of 100 nM purified His-PARS1 (1001–1512 aa) WT or mutants. After 5 min, the reaction mixture was quenched on Whatman filter paper presoaked with 5% trichloroacetic acid (TCA). The filter papers were washed three times in 5% TCA for 10 min at 4 °C and once in 100% ethanol for 10 min. The filter papers were dried and radioactivity was quantified using liquid scintillation counter (LSC).

**Immunoprecipitation assay.** For the detection of interaction between EPRS1 and TβRI, cells were lysed with lysis buffer containing 50 mM Tris-HCl (pH 7.4), 150 mM NaCl, 0.5% Triton X-100, 0.5% NP-40, 1 mM EDTA, 1 mM EGTA and protease inhibitor. Cell lysates were pre-incubated with protein A agarose (Invitrogen, 15918014) for an hour at 4 °C with rotation to eliminate nonspecific binding to the beads. The precleared cell lysates were incubated with anti-TβRI antibody for overnight at 4 °C with rotation.

**TABLE 4** Reagents used in this study

| Name of reagent | Source | Catalog number |
|---|---|---|
| TGF-β | R&D systems | 240-B-002 |
| Cycloheximide | Sigma-Aldrich | C4859 |
| MG-132 | Sigma-Aldrich | M7449 |
| 5Z-7-Oxozeaenol | Sigma-Aldrich | O9890 |
| U0126 | Sigma-Aldrich | U120 |
| SB202190 | Sigma-Aldrich | S7067 |
| Doxycycline | Sigma-Aldrich | D9891 |
| JNK inhibitor II | Calbiochem | 420119 |
| Puromycin | CLN | Z1305N |
| Protease inhibitor cocktail | Roche | 11 836 153 001 |
| Phosphatase inhibitor cocktail | Thermo Fisher Scientific | 78423 |
| His-TAK-TAB1 fusion protein | Merck Millipore | 14-600 |
| Halofuginone hydrobromide | Sigma-Aldrich | 32481-10MG |
| Borrelidin | Sigma-Aldrich | B3061-1MG |
| ATP disodium salt hydrate | Sigma-Aldrich | A26209-5G |
| tRNA from baker's yeast | Sigma-Aldrich | 10109495001 |
| L-[2,3,4,5-$^{3}$H]-Proline | Perkin Elmer | NET483005MC |
| [γ-$^{32}$P]-ATP | PerkinElmer | NEG002A250UC |
| Ni-NTA Agarose | QIAGEN | 30230 |
| Glutathione Sepharose 4B | GE Healthcare | 17-0756-01 |
| rProtein G Agarose | Invitrogen | 15920-010 |
| 4% Paraformaldehyde solution | Boster Bio | AR1068 |
| CAS-block™ histochemical reagent | Thermo Fisher Scientific | 008120 |
| Hoechst 33342, trihydrochloride, trihydrate | Thermo Fisher Scientific | H3570 |

Then, protein A agarose was added to the samples and incubated for 2 h at 4 °C with rotation. The beads were washed three times with washing buffer 1 (50 mM Tris-HCl (pH 7.4), 150 mM NaCl, 0.5% Triton X-100, 0.5% NP-40) and twice with washing buffer 2 (50 mM Tris-HCl (pH 7.4), 150 mM NaCl). Coprecipitated proteins were dissolved in SDS sample buffer, denatured for 5 min at 100 °C, and then separated through SDS-PAGE.

**Magnetic bead pull-down assay.** HEK293T cells were cotransfected with Strep-EPRS1 and each of Flag-TβRI, TβRII, GFP-SMAD2, SMAD3, SMAD4, or SMAD7 were lysed with lysis buffer (20 mM Tris-HCl (pH 7.4), 150 mM NaCl, 0.5% Triton X-100, 0.5% NP-40, 1 mM EDTA, 1 mM EGTA, and protease inhibitor). Cell lysates were incubated with MagStrep type3 XT beads (IBA life sciences, 2-4090-002) for an hour at 4 °C with rotation. Then, the beads were washed three times with the wash buffer 1 (50 mM Tris-HCl (pH 7.4), 150 mM NaCl, 0.5% Triton X-100, 0.5% NP-40) by short vortex. Coprecipitated proteins were dissolved in the SDS sample buffer, denatured for 5 min at 100 °C and separated in the magnetic separator. The supernatants were then subjected to SDS-PAGE.

**In vitro binding assay.** BL21 strain was transformed by GST-EV, GST-TβRI plasmids and protein expression was induced by supplementation with 1 mM isopropyl-β-D-thiogalactopyranoside for 16 h at 18 °C. The cells were lysed by sonication and then purified using glutathione Sepharose® 4B bead (GE Healthcare, 17-0756-01). For binding assay, 5 μg of GST-tagged proteins were incubated with 500 ng of His-tagged PARS1 proteins in the absence or presence of 1 μM HF in binding buffer containing 50 mM Tris-HCl (pH 7.4), 150 mM NaCl, 0.5% Triton X-100, 0.5% NP-40, 1 mM EDTA, 1 mM EGTA and protease inhibitor for 6 h at 4 °C with rotation. The beads were washed three times with the wash buffer 1 (50 mM Tris-HCl (pH 7.4), 150 mM NaCl, 0.5% Triton X-100 and 0.5% NP-40), and then twice with the wash buffer 2 (50 mM Tris-HCl (pH 7.4) and 150 mM NaCl). Coprecipitated His-PARS1 were dissolved in SDS sample buffer, denatured for 5 min at 100 °C, and then separated through SDS-PAGE.

**Immunoblot assay.** Cells were lysed with lysis buffer (50 mM Tris-HCl (pH 7.4),150 mM NaCl, 0.5% Triton X-100, 0.05% SDS, 1 mM EDTA, 1 mM EGTA and protease inhibitor) and collected in a 1.5 mL tube and then incubated at 4 °C with gentle agitation for 20 min. The tubes were centrifuged at 12,700 rpm for 15 min at 4 °C and supernatants were collected and protein concentrations were quantified using Bradford reagent. Samples were denatured by adding SDS sample buffer and boiled at 100 °C for 5 min. The samples were separated by SDS-PAGE, transferred to PVDF membrane. The membrane was blocked and incubated with specific antibodies. After rinsing with TBS-T (Tris-based saline with 0.05% Tween 20) three times the membrane was incubated with horseradish peroxidase-coupled anti-mouse or anti-rabbit IgG secondary antibodies. Signals were developed using Amersham ECL Prime (Cytiva).

**Subcellular fractionation.** The cells were separated to membrane, cytosolic and nuclear fractions using Proteoextract kit (Calbiochem, 539790) following the manufacturer's instructions.

**Collagen gel contraction assay.** Cell suspension were prepared ($1.5 \times 10^5$ cells/mL) and 400 μL cell suspensions were mixed with the 100 μL of 3 mg/mL collagen solution (Corning, 354236). Then, appropriate volume of 1 M NaOH was added to the mixture to adjust to neutral pH. The mixture was

transferred to 24-well plates and incubated at 37 °C in 5% $CO_2$ incubator. Gel area was quantified using ImageJ.

**In vitro kinase assay.** To prepare substrates for *in vitro* kinase assay, HEK293T cells were transfected with empty vector or Strep-EPRS1 and pulled down using MagStrep type3 XT beads. After the beads were pre-incubated with active TAK1-TAB1 fusion protein (Thermo Scientific, PV4394) for 5 min at 4 °C in kinase assay buffer (25 mM MOPS (pH 7.2), 0.25 mM dithiothreitol, 25 mM $MgCl_2$, 12.5 mM β-glycerophosphate, 2 mM EDTA, 5 mM EGTA and phosphatase inhibitor cocktail). The reaction was started by adding [$\gamma$-$^{32}$P] ATP 10 μCi (3000 Ci/mmol) and the samples were incubated for 15 min at 30 °C. The reaction was terminated using SDS sample buffer, followed by denaturation for 5 min at 100 °C. Phosphorylated proteins were separated by SDS-PAGE. The gel was stained using Coomassie brilliant blue reagent and then dried. Radioactive isotope labelled protein band was detected by autoradiography (FUJIFILM, FLA-3000).

**Immunofluorescence staining.** LX-2 cells ($5 \times 10^4$ cells/well) were seeded on the cover slip placed in the 12 well plate. After 24 h, the cells were starved of serum for 17 h and incubated in the presence or absence of TGF-β for 20 min. Cells were rinsed twice with cold PBS and then incubated with permeabilization solution (20 μg/mL digitonin and protease inhibitor in PBS) with shaking for 5 min. After rinsing twice with cold PBS, cells were fixed with 4% paraformaldehyde for 10 min. After rinsing twice with cold PBS, the cover slips were incubated with CAS-Block for 15 min at 26 °C for blocking. For staining, the cover slips were incubated with anti-EPRS1 antibody (1:1000) and anti-pan-cadherin antibody (1:100) for 2 h at 26 °C, rinsed three times with PBS, incubated with anti-rabbit and anti-mouse secondary antibodies that are conjugated with Alexa Fluor 647 and 488, respectively, for 1 h at 26 °C, rinsed three times with PBS, incubated with Hoechst (1:500) for 10 min at room temperature, rinsed three times with PBS, and mounted on slide glass. The samples were observed using confocal laser scanning microscope (Nikon, A1Rsi).

**Cloning, expression, and purification of EARS1 and WHEP + PARS1.** Each cDNA of EARS1 (194–709) and WHEP + PARS1 (747–1512) was cloned into pET28a (Novagen) and transformed into *Escherichia coli* Rosetta 1 (DE3) (Novagen). Each cell was cultivated at 37 °C in Luria–Bertani medium until 0.6–0.8 optical density at 600 nm. The recombinant proteins were induced by the addition of 0.5 mM isopropyl-β-D-1-thiogalactopyranoside at 18 °C for 18 h. The cells were harvested by centrifugation at 4000 *g* for 20 min at 4 °C. The cell pellet of EARS1 was resuspended in Buffer A (20 mM Tris (pH 8.0), 150 mM NaCl) and that of WHEP + PARS1 was resuspended in Buffer B (20 mM Tris (pH 8.0), 100 mM NaCl, 5 mM $MgCl_2$). After sonication of the cell resuspensions and centrifugation at 25,000 *g* for 1 h at 4 °C, soluble fractions of the proteins were obtained. The supernatants were filtered using 0.45 μm membrane and put onto $Ni^{2+}$-affinity columns that were equilibrated by Buffer A. Recombinant proteins attached to the column were eluted with 500 mM imidazole in Buffer A. Pooled fractions of EARS1 and WHEP + PARS1 were diluted 10 times with Buffer C (20 mM Tris (pH 8.0), 150 mM NaCl, and 500 mM imidazole) and Buffer D (20 mM Tris (pH 8.0), 150 mM NaCl, 5 mM $MgCl_2$ and 500 mM imidazole), respectively. After purified by anion exchange chromatography employing a linear gradient of 1 M NaCl for EARS1; 1 M NaCl and 5 mM DTT for WHEP + PARS1, the proteins were applied to a HiLoad 26/60 Superdex 200 prep-grade column for size-exclusion chromatography in final buffer (20 mM Tris (pH 8.0), 150 mM NaCl for EARS1, and 20 mM Tris (pH 8.0), 150 mM NaCl, 5 mM $MgCl_2$ and 1% glycerol for WHEP + PARS1). The recombinant protein fractions were pooled and concentrated to 15 mg/mL (EARS1) and 42 mg/mL (WHEP + PARS1) using an Amicon® Ultra Centrifugal Filter (Merck Millipore, GE), respectively, and stored at −80 °C.

**Binding affinity measurement by microscale thermophoresis (MST).** MST assays were conducted using a NanoTemper Technologies Monolith NT.115.[45,46] PARS1 was labeled with fluorescence (Monolith His-Tag Labeling Kit RED-tris-NTA second generation). To obtain titration curve, 16 different concentrations of TβRI were prepared by 2-fold serial dilution of 85 μM TβRI and incubated with 200 nM fluorescence-tagged PARS1 in PBS supplemented with 0.05% (w/v) Tween-20 and 0.05% BSA. The samples were loaded into high-precision capillaries (Monolith NT.115 Capillaries) and the normalized fluorescence readings (thermophoresis plus T-jump) were plotted as a function of analyte concentration. NanoTemper software was used to fit the curves and figure out the dissociation constant $K_d$.

## FUNDING

This work was supported by the National Research Foundation (NRF) grant funded by the Korean government (MSIT) [2021R1C1C1013332, 2021R1A3B1076605, and 2022R1I1A1A01068223] and by the Yonsei University Research Fund [2020-22-0358, 2020-22-0356 and 2021-22-0061].

## ORCID

Sunghoon Kim http://orcid.org/0000-0002-1570-3230

## DATA AVAILABILITY STATEMENT

Data are available at Mendeley: EPRS1 Controls the TGF-β Signaling Pathway via Interaction with TβRI in Hepatic Stellate Cell (DOI: 10.17632/wxfrdhmc6x.1).

## REFERENCES


1. Hernandez-Gea V, Friedman SL. Pathogenesis of liver fibrosis. Annu Rev Pathol. 2011;6:425–456. doi:10.1146/annurev-pathol-011110-130246.
2. Kisseleva T, Brenner D. Molecular and cellular mechanisms of liver fibrosis and its regression. Nat Rev Gastroenterol Hepatol. 2021;18:151–166. doi:10.1038/s41575-020-00372-7.
3. Wang S, Friedman SL. Hepatic fibrosis: a convergent response to liver injury that is reversible. J Hepatol. 2020;73:210–211. doi:10.1016/j.jhep.2020.03.011.
4. Higashi T, Friedman SL, Hoshida Y. Hepatic stellate cells as key target in liver fibrosis. Adv Drug Deliv Rev. 2017;121:27–42. doi:10.1016/j.addr.2017.05.007.
5. Stefanovic B, Hellerbrand C, Holcik M, Briendl M, Aliebhaber S, Brenner DA. Posttranscriptional regulation of collagen alpha1(I) mRNA in hepatic stellate cells. Mol Cell Biol. 1997;17:5201–5209. doi:10.1128/MCB.17.9.5201.
6. Batlle E, Massague J. Transforming growth factor-beta signaling in immunity and cancer. Immunity. 2019;50:924–940. doi:10.1016/j.immuni.2019.03.024.
7. Massague J. TGFbeta signalling in context. Nat Rev Mol Cell Biol. 2012;13:616–630. doi:10.1038/nrm3434.
8. Lonn P, Moren A, Raja E, Dahl M, Moustakas A. Regulating the stability of TGF beta receptors and smads. Cell Res. 2009;19:21–35. doi:10.1038/cr.2008.308.
9. Miyazawa K, Miyazono K. Regulation of TGF-beta family signaling by inhibitory smads. Csh Perspect Biol. 2017;9:a022095.
10. Kim S, You S, Hwang D. Aminoacyl-tRNA synthetases and tumorigenesis: more than housekeeping. Nat Rev Cancer. 2011;11:708–718. doi:10.1038/nrc3124.
11. Kwon NH, Fox PL, Kim S. Aminoacyl-tRNA synthetases as therapeutic targets. Nat Rev Drug Discov. 2019;18:629–650. doi:10.1038/s41573-019-0026-3.
12. Sung Y, Yoon I, Han JM, Kim S. Functional and pathologic association of aminoacyl-tRNA synthetases with cancer. Exp Mol Med. 2022;54:553–566. doi:10.1038/s12276-022-00765-5.
13. Khan K, Baleanu-Gogonea C, Willard B, Gogonea V, Fox PL. 3-Dimensional architecture of the human multi-tRNA synthetase complex. Nucleic Acids Res. 2020;48:8740–8754. doi:10.1093/nar/gkaa569.
14. Kim JY, Kang YS, Lee JW, Kim HJ, Ahn YH, Park H, Ko YG, Kim S. P38 is essential for the assembly and stability of macromolecular tRNA synthetase complex: implications for its physiological significance. Proc Natl Acad Sci U S A. 2002;99:7912–7916. doi:10.1073/pnas.122110199.
15. Park SG, Choi EC, Kim S. Aminoacyl-tRNA synthetase-interacting multifunctional proteins (AIMPs): a triad for cellular homeostasis. IUBMB Life. 2010;62:296–302. doi:10.1002/iub.324.
16. Kim DG, Choi JW, Lee JY, Kim H, Oh YS, Lee JW, Tak YK, Song JM, Razin E, Yun SH, et al. Interaction of two translational components, lysyl-tRNA synthetase and p40/37LRP, in plasma membrane promotes laminin-dependent cell migration. Faseb J. 2012;26:4142–4159. doi:10.1096/fj.12-207639.
17. Kwon NH, Kang T, Lee JY, Kim HH, Kim HR, Hong J, Oh YS, Han JM, Ku MJ, Lee SY, et al. Dual role of methionyl-trna synthetase in the regulation of translation and tumor suppressor activity of aminoacyl-tRNA synthetase-interacting multifunctional protein-3. Proc Natl Acad Sci U S A. 2011;108:19635–19640. doi:10.1073/pnas.1103922108.
18. Sampath P, Mazumder B, Seshadri V, Gerber CA, Chavatte L, Kinter M, Ting SM, Dignam JD, Kim S, Driscoll DM, et al. Noncanonical function of glutamyl-prolyl-tRNA synthetase: gene-specific silencing of translation. Cell. 2004;119:195–208. doi:10.1016/j.cell.2004.09.030.
19. Jiang S, Zeng Q, Gettayacamin M, Tungtaeng A, Wannaying S, Lim A, Hansukjariya P, Okunji CO, Zhu S, Fang D. Antimalarial activities and therapeutic properties of febrifugine analogs. Antimicrob Agents Chemother. 2005;49:1169–1176. doi:10.1128/AAC.49.3.1169-1176.2005.
20. Assis PA, De Figueiredo-Pontes LL, Lima AS, Leao V, Candido LA, Pintao CT, Garcia AB, Saggioro FP, Panepucci RA, Chahud F, et al. Halofuginone inhibits phosphorylation of Smad-2 reducing angiogenesis and leukemia burden in an acute promyelocytic leukemia mouse model. J Exp Clin Cancer Res. 2015;34:65. doi:10.1186/s13046-015-0181-2.
21. Granot I, Bartov I, Plavnik I, Wax E, Hurwitz S, Pines M. Increased skin tearing in broilers and reduced collagen synthesis in skin in vivo and in vitro in response to the coccidiostat halofuginone. Poult Sci. 1991;70:1559–1563. doi:10.3382/ps.0701559.
22. Granot I, Halevy O, Hurwitz S, Pines M. Halofuginone: an inhibitor of collagen type I synthesis. Biochim Biophys Acta. 1993;1156:107–112. doi:10.1016/0304-4165(93)90123-p.
23. Pines M, Nagler A. Halofuginone: a novel antifibrotic therapy. Gen Pharmacol. 1998;30:445–450. doi:10.1016/s0306-3623(97)00307-8.
24. Sundrud MS, Koralov SB, Feuerer M, Calado DP, Kozhaya AE, Rhule-Smith A, Lefebvre RE, Unutmaz D, Mazitschek R, Waldner H, et al. Halofuginone inhibits TH17 cell differentiation by activating the amino acid starvation response. Science. 2009;324:1334–1338. doi:10.1126/science.1172638.
25. Keller TL, Zocco D, Sundrud MS, Hendrick M, Edenius M, Yum J, Kim YJ, Lee HK, Cortese JF, Wirth DF, et al. Halofuginone and other febrifugine derivatives inhibit prolyl-tRNA synthetase. Nat Chem Biol. 2012;8:311–317. doi:10.1038/nchembio.790.
26. Son J, Lee EH, Park M, Kim JH, Kim J, Kim S, Jeon YH, Hwang KY. Conformational changes in human prolyl-tRNA synthetase upon binding of the substrates proline and ATP and the inhibitor halofuginone. Acta Crystallogr D Biol Crystallogr. 2013;69:2136–2145. doi:10.1107/S0907444913020556.
27. Zhou H, Sun L, Yang XL, Schimmel P. ATP-directed capture of bioactive herbal-based medicine on human trna synthetase. Nature. 2013;494:121–124. doi:10.1038/nature11774.
28. Song DG, Kim D, Jung JW, Nam SH, Kim JE, Kim HJ, Kim JH, Lee SJ, Pan CH, Kim S, et al. Glutamyl-prolyl-tRNA synthetase induces fibrotic extracellular matrix via both transcriptional and translational mechanisms. FASEB J. 2019;33:4341–4354. doi:10.1096/fj.201801344RR.
29. Song DG, Kim D, Jung JW, Nam SH, Kim JE, Kim HJ, Kim JH, Pan CH, Kim S, Lee JW. Glutamyl-prolyl-tRNA synthetase regulates epithelial expression of mesenchymal markers and extracellular matrix proteins: Implications for idiopathic pulmonary fibrosis. Front Pharmacol. 2018;9:1337. doi:10.3389/fphar.2018.01337.
30. Wu JB, Subbaiah KCV, Xie LHT, Jiang F, Khor ES, Mickelsen D, Myers JR, Tang WHW, Yao P. Glutamyl-prolyl-tRNA synthetase regulates proline-rich pro-fibrotic protein synthesis during cardiac fibrosis. Circ Res. 2020;127:827–846. doi:10.1161/CIRCRESAHA.119.315999.
31. Hinz B, Celetta G, Tomasek JJ, Gabbiani G, Chaponnier C. Alpha-smooth muscle actin expression upregulates fibroblast contractile activity. Mol Biol Cell. 2001;12:2730–2741. doi:10.1091/mbc.12.9.2730.
32. Ninomiya-Tsuji J, Kajino T, Ono K, Ohtomo T, Matsumoto M, Shiina M, Mihara M, Tsuchiya M, Matsumoto K. A resorcylic acid lactone, 5z-7-oxozeaenol, prevents inflammation by inhibiting the catalytic activity of TAK1 MAPK kinase kinase. J Biol Chem. 2003;278:18485–18490. doi:10.1074/jbc.M207453200.
33. Sakurai H, Nishi A, Sato N, Mizukami J, Miyoshi H, Sugita T. TAK1-TAB1 fusion protein: a novel constitutively active mitogen-activated protein kinase kinase kinase that stimulates AP-1 and NF-kappaB signaling pathways. Biochem Biophys Res Commun. 2002;297:1277–1281. doi:10.1016/s0006-291x(02)02379-3.
34. Lee EY, Lee HC, Kim HK, Jang SY, Park SJ, Kim YH, Kim JH, Hwang J, Kim JH, Kim TH, et al. Infection-specific phosphorylation of glutamyl-prolyl tRNA synthetase induces antiviral immunity. Nat Immunol. 2016;17:1252–1262. doi:10.1038/ni.3542.
35. Fang P, Yu X, Jeong SJ, Mirando A, Chen K, Chen X, Kim S, Francklyn CS, Guo M. Structural basis for full-spectrum inhibition of translational functions on a tRNA synthetase. Nat Commun. 2015;6:6402. doi:10.1038/ncomms7402.
36. Jeong SJ, Kim JH, Lim BJ, Yoon I, Song JA, Moon HS, Kim D, Lee DK, Kim S. Inhibition of muc1 biosynthesis via threonyl-trna synthetase suppresses pancreatic cancer cell migration. Exp Mol Med. 2018;50:e424. doi:10.1038/emm.2017.231.
37. Tan Z, Sun H, Xue T, Gan C, Liu H, Xie Y, Yao Y, Ye T. Liver fibrosis: therapeutic targets and advances in drug therapy. Front Cell Dev Biol. 2021;9:730176. doi:10.3389/fcell.2021.730176.
38. Liang J, Zhang B, Shen RW, Liu JB, Gao MH, Li Y, Li YY, Zhang W. Preventive effect of halofuginone on concanavalin a-induced liver fibrosis. PloS One. 2013;8:e82232. doi:10.1371/journal.pone.0082232.
39. Pines M, Knopov V, Genina O, Lavelin I, Nagler A. Halofuginone, a specific inhibitor of collagen type I synthesis, prevents dimethylnitrosamine-induced liver cirrhosis. J Hepatol. 1997;27:391–398. doi:10.1016/s0168-8278(97)80186-9.
40. Tan S, Zhao J, Sun Z, Cao S, Niu K, Zhong Y, Wang H, Shi L, Pan H, Hu J, et al. Hepatocyte-specific tak1 deficiency drives RIPK1 kinase-dependent inflammation to promote liver fibrosis and hepatocellular carcinoma. Proc Natl Acad Sci U S A. 2020;117:14231–14242. doi:10.1073/pnas.2005353117.
41. Schnabl B, Bradham CA, Bennett BL, Manning AM, Stefanovic B, Brenner DA. TAK1/JNK and p38 have opposite effects on rat hepatic stellate cells. Hepatology. 2001;34:953–963. doi:10.1053/jhep.2001.28790.

42. Mochizuki T, Miyazaki H, Hara T, Furuya T, Imamura T, Watabe T, Miyazono K. Roles for the MH2 domain of Smad7 in the specific inhibition of transforming growth factor-beta superfamily signaling. J Biol Chem. 2004;279:31568–31574. doi:10.1074/jbc.M313977200.
43. Wu JW, Hu M, Chai J, Seoane J, Huse M, Li C, Rigotti DJ, Kyin S, Muir TW, Fairman R, et al. Crystal structure of a phosphorylated Smad2. Recognition of phosphoserine by the MH2 domain and insights on smad function in TGF-beta signaling. Mol Cell. 2001;8:1277–1289. doi:10.1016/s1097-2765(01)00421-x.
44. Nakashima K, Yanagisawa M, Arakawa H, Kimura N, Hisatsune T, Kawabata M, Miyazono K, Taga T. Synergistic signaling in fetal brain by STAT3-Smad1 complex bridged by p300. Science. 1999;284:479–482. doi:10.1126/science.284.5413.479.
45. Bartoschik T, Galinec S, Kleusch C, Walkiewicz K, Breitsprecher D, Weigert S, Muller YA, You C, Piehler J, Vercruysse T, et al. Near-native, site-specific and purification-free protein labeling for quantitative protein interaction analysis by microscale thermophoresis. Sci Rep. 2018;8:4977. doi:10.1038/s41598-018-23154-3.
46. Wienken CJ, Baaske P, Rothbauer U, Braun D, Duhr S. Protein-binding assays in biological liquids using microscale thermophoresis. Nat Commun. 2010;1:100. doi:10.1038/ncomms1093.